Homogeneous Nucleation in Metal Vapors. 3. Temperature Dependence of the Critical Supersaturation Ratio for Iron, Lead, and Bismuth

D. J. Frurip and S. H. Bauer*

Department of Chemistry, Cornell University, Ithaca, New York 14853 *(Received July 19, 1976; Revised Manuscript Received March 7, 1977)*

The temperature dependence of the critical supersaturation ratio was measured for the onset of very rapid condensation from the vapors to "liquid" clusters for iron, lead, and bismuth. Controlled supersaturation levels were generated by shock heating corresponding organometallics, highly diluted in argon. Both incident and reflected shock regimes were used. While the conditions for attaining criticality differed markedly for the two modes of operation, the two sets of data check quite well. We demonstrated that even though the experiments are inherently subject to substantial random errors, none of the current theories for homogeneous nucleation satisfactorily predict, to within generously allocated error limits, the observed $S_c(T)$. Empirically the data are best represented by functions of the form $S_c(T) = 10^2 a \exp(-10^{-3} bT, \mathrm{K})$ with $0.7 \leq a \leq 2$ and $1.5 \leq b \leq 3.5$. We conclude that in view of the concurrent ambiguities in the magnitudes of the *assumed* flux currents and the dependence of the surface tension on temperature, one may question whether determination of $S_c(T)$ can provide a meaningful test for the classical theories of condensation.

Introduction

This is a brief report on the determination of critical supersaturation ratios for avalanche condensation from the vapors of iron, lead, and bismuth, and of their dependence on the temperature. Our experimental approach [developed by Kung and Bauer,[1] and Homer and Prothero[2]] consisted of shock heating gaseous organometallics [$Fe(CO)_5$, $Pb(CH_3)_4$, and $Bi(CH_3)_3$] to temperatures such that all the ligands were stripped from the central metal atom within a few microseconds after passage of the shock front. Specified supersaturation levels with respect to the metal atoms were thus produced. The onset of condensation under essentially isothermal conditions was monitored by measuring the attenuation of an unpolarized He–Ne laser beam, as a function of time. A listing of the requisite turbidity equations is given below.

In a system which is sufficiently dilute, so that multiple scattering can be neglected, and the scattering-absorbing particles are randomly positioned, the transmitted intensity of monochromatic radiation is $I = I_0 \exp(-\tau l)$, where τ is the "turbidity", expressed in terms of $\tau = NC_{ext}$; N is the number density of particles, and C_{ext} is an extinction cross section. From Mie's full solution for small absorbing spheres[3] [$\lambda >>$ mean diameter], for unpolarized incident radiation

$$C_{ext} = -\frac{6\pi\langle v\rangle}{\lambda} I_m\left[\frac{m^2-1}{m^2+2}\right] \qquad (1)$$

where $\langle v\rangle$ is the mean particle volume, $\langle v\rangle = \int vP(v)\,dv$; $P(v)$ is the normalized distribution function, and m is the complex index of refraction [$m \equiv n' - iq$]. Hence, for a condensing system, where the density of particles is changing and unknown, turbidity measurements alone are insufficient to determine particle sizes. However, it has been shown[4] that the recorded turbidity signal, $(I_0 - I)$, is directly proportional to the mass fraction of the metal condensed. Since the nucleation rate is extremely sensitive to the supersaturation ratio, S, it is expected and experimentally confirmed that $(I_0 - I)$ shows a very fast rise for high S, once condensation starts. As the supersaturation ratio is reduced, the nucleation rate decreases rapidly and approaches zero at the critical S_c. Then the transmitted signal shows little deviation from the initial light level.

TABLE I: Equilibrated Species Considered in NASA Program

Precursor	Equilibrated species (gaseous)
$Fe(CO)_5$	$Fe(CO)_5$, Fe, CO, Ar
$Pb(CH_3)_4$	$Pb(CH_3)_4$, Pb, CH_3, CH_2, CH, H_2, C_2H_6, C_2H_4, CH_4, Ar
$Bi(CH_3)_3$	$Bi(CH_3)_3$, Bi, CH_3, CH_2, CH, H_2, C_2H_6, C_2H_4, CH_4, Ar

Detailed descriptions of the operation of shock tubes and the appropriate gas dynamic relations are given in standard texts.[5] To compute the temperature of the shock heated gas from the measured shock velocity, one must specify the thermodynamic state of the gas sample immediately after passage through the "shock front". In these studies one must adjust conditions so that dissociation of the metal bearing compound occurs very quickly compared to the subsequent condensation kinetics. To select appropriate shock parameters, we used the NASA "equilibrium shock" program.[6] Standard enthalpies of formation, standard entropies, the initial concentration of the parent compound, and appropriate heat capacity data must be inserted as parameters to perform the calculations. The temperature dependent free energy functions for all the product species must also be included. The species which we assumed to have attained equilibrium are listed in Table I.

No rate data are available for the unimolecular decomposition of $Fe(CO)_5$. By analogy with similar compounds, such as $Ni(CO)_4$, the rate is presume to be very fast at shock temperatures, 1500–2500 K.[1,7] We estimate that at 1500 K the half-life for the complete stripping of the CO groups is less than 1 ns. Vapor pressure data[8] for Fe and $Fe(CO)_5$ indicate that a sample of $Fe(CO)_5$ can be prepared at room temperature such that under typical incident shock conditions the concentration of Fe atoms is sufficiently supersaturated to condense. Experiments showed that at moderate supersaturation, the time for complete condensation of the Fe vapor was of the order of 50 μs. The experimental requirements are therefore met for $Fe(CO)_5$ at temperatures greater than 1500 K.

The Journal of Physical Chemistry, Vol. 81, No. 10, 1977

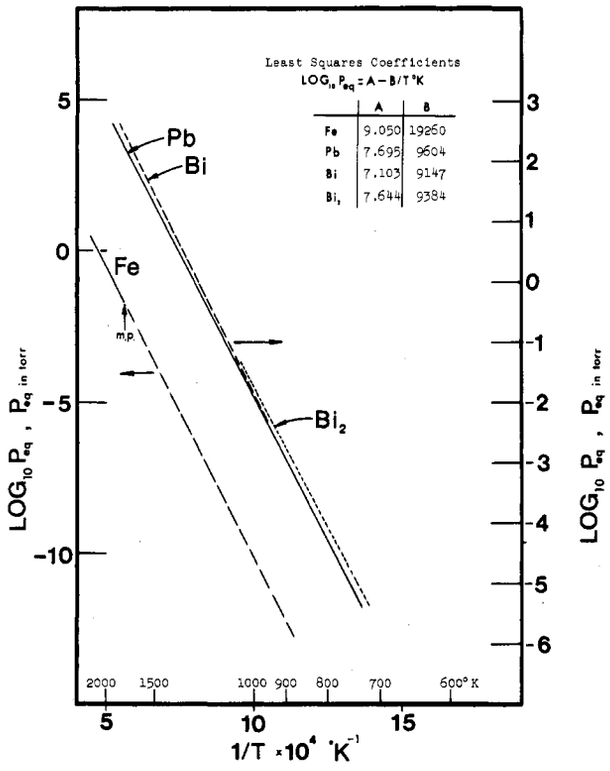

Figure 1. Vapor pressure data.

Homer and Hurle[9] measured the rate of decomposition of $Pb(CH_3)_4$ over the temperature range 890–1060 K, and found for the unimolecular rate constant

$$\log k_{TML} = (13.25 \pm 0.4) - (9.0 \pm 0.4) \times 10^3/T \text{ K} \quad (2)$$

As in the case of $Fe(CO)_5$, the removal of the first CH_3 group was assumed to be rate limiting and that the subsequent stripping of the remaining methyl groups occurs much faster. They noted that there were no reports of stable intermediate lead–methyl radicals. As will be described below, the time for complete condensation of lead at supersaturations near critical was experimentally determined to be of the order of 300 μs. Hence at least 90% of the TML should be decomposed within about one third of that time after passage of the shock front. By setting $t_{90\%} = \ln(10)/k_{TML} = 100$ μs we find that this condition is met for temperatures above 980 K. Vapor pressure data for Pb (Figure 1) show that large supersaturation ratios can easily be obtained at these temperatures for a dilute mixture (≈1%) of the TML in Ar. Thus, the experimental requirements are also met for TML, as long as the shocked gas temperature is above 980 K. The methyl radicals recombine rapidly to produce $C_2H_6(g)$, $C_2H_4(g) + H_2(g)$, and $CH_4(g) + CH_2(g)$, etc. These species, along with TML(g), $CH_3(g)$, Pb(g), and Ar(g), were considered to be in thermal equilibrium for calculating the shocked gas temperature (Table I).

Price et al.[10] determined the rate of decomposition of trimethylbismuth (TMB) over the temperature range 600–900 K, by measuring yields of $CH_4(g)$ and $C_2H_6(g)$ [H_2 and C_2H_4 were also observed but in minute amounts]. They observed that total decomposition to the free metal and methyl groups was fast relative to the initial bond rupture, and report for the unimolecular rate constant

$$\log k_{TMB} = 14.0 - 9.61 \times 10^3/T \text{ K} \quad (3)$$

As does TML, within 150 μs, 90% of TMB is decomposed at a temperature of 980 K. However, we decided to use an alternate technique for bismuth, as outlined below.

Experiments with reflected shocks, the technique developed by Kung and Bauer,[4] have two advantages: (1) the temperature range can be extended to lower values, and (2) the efficiency of data collection is considerably increased since a determination of $S_c(T)$ is obtained per successful run. The shock tube was *tuned* so that the reflected shock, head of the expansion fan, and contact surface met at approximately the same position in the shock tube. The net result is an exponential decay of temperature and pressure after a specified dwell time. The elevated temperature and relatively long residence time in the reflected shock regime results in rapid and complete decomposition of the TMB to generate an *undersaturated* vapor. However, after the expansion wave cools the shock heated gas the level of supersaturation rises, and eventually the Bi vapor becomes critically supersaturated and condensation sets in. With the NASA program one may calculate conditions in the expansion wave at the critical *take-off point*, using the instantaneous pressure, as measured by the piezoelectric sensor. The corresponding temperature in the expansion wave is given by the adiabatic relation

$$T_5/T_{5e} = (P_5/P_{5e})^{\gamma_5^{-1}/\gamma_5} \quad (4)$$

where the subscripts 5 and 5e refer to the reflected shock and expansion waves, respectively. For dilute samples, the heat capacity ratio, γ_5, is that of the inert gas diluent. Since the critical supersaturation condition is attained in every run, one $S_c(T)$ point is observed in every experiment. To obtain data over a wider range of temperatures, one need only vary the initial pressure of the test gas or change the sample composition.

Experimental Section

Sample Preparation. Samples of the metalloorganics $Fe(CO)_5$, $Pb(CH_3)_4$, and $Bi(CH_3)_3$ were purified and diluted in argon, to concentrations 0.1–2.0 mol %; ultra-high-purity argon (99.999%) was used as a diluent. The mixtures were allowed to stand for a minimum of 24 h before use. The metal bearing compounds, all liquids with appreciable vapor pressures at room temperature, were obtained from Alfa Inorganics Co. The $Fe(CO)_5$ was doubly distilled and only the middle fraction was used in preparing the sample. The suppliers indicated that the $Bi(CH_3)$ was pure; it was used without further purification except for repeated freezing and outgassing. The $Pb(CH_3)_4$ was obtained as an 80% solution in toluene. This was purified to 99.5 ± 0.2% on a Hewlett Packard Model 700 gas chromatograph, using a 6-ft 10% Carbowax 20M prep-column. Adequate resolution of the toluene and TML peaks was available at a column temperature of 150 °C. During the latter stages of the experiments we obtained pure TML from the ROC-RIC Co. The experimental results remained unchanged.

The Shock Tube. A detailed description of the 1.5-in. brass shock tube used in this experiment has been published.[11] The length of the driver section was 4 ft; the test section was 13 ft long for the incident shock experiments, but was shortened to 10.5 ft for the reflected shock experiments. Lucite windows (1 in.) were mounted flush with the inside walls 10 ft 4 in. downstream from the diaphragm. The shock tube was operated in the single pulse mode using a 3.28×10^4 cm^3 dump tank. The diaphragms were mylar and ranged in thickness from 0.5 to 5 mil. Pure He or mixtures of He and N_2 were used as driver gases. A barium titanate pressure transducer upstream from the window actuated the electronics. Four platinum film gauges were used for measuring shock speeds. The output

from the gauges was amplified and fed into a Tektronix Model 535 oscilloscope, modified to provide 10 μs time marks to the raster display. Pressure history was monitored with a Kistler No. 610 quartz pressure transducer located immediately above the observation windows. The tube leak-outgassing rate was 0.5 mTorr/min.

Optical Arrangement. An unpolarized 1.5-mW Edmund Scientific He–Ne laser (6328 Å) was directed through the center of the shock tube windows. Care was taken to direct the incident and transmitted beams normal to the windows; this ensured that the beam was also perpendicular to the flow. At a distance of about 2.5 cm from the exit window, the beam passed through an adjustable iris which was set to be slightly larger than the beam diameter at that point (2 mm). An EMI-9634 phototube was located 1 m from the exit window; it had a $(1/e)$ rise time of 3.0 μs. The entrance to the phototube was masked with a 6328 ± 2 Å interference filter, and a ground glass diffuser. There are no Ar, Bi, Pb, Fe, Hg, or Na emission lines in the range 6328 ± 2 Å. The combination of the iris plus the relatively large distance between the phototube and the shock tube ensured that a negligible amount of black-body radiation from the condensing particles reached the detector. The phototube output (with the laser off), for every metal studied, showed no significant intensity from thermal emission. The output from the phototube was monitored simultaneously with the output from the pressure transducer on a Tektronix Model 502 dual beam oscilloscope. This allowed us to determine the exact shock arrival time in the incident shock experiments. In studies with reflected shocks this recorded the pressure history throughout the entire experiment and the essential data for calculating the temperature of the gas at the turbidity take-off point.

The powder that settled inside the tube was analyzed via powder x-ray diffraction. The results confirmed the presence of crystallites of the several metals. In addition, an analysis of the diffraction line widths gave crystallite sizes which agreed with an electron microscopic examination of particle sizes. To prevent any heterogeneous nucleation on the metal particles attached to the walls, the tube was thoroughly cleaned after each run with a cheesecloth swab moistened with ethanol.

Data Reduction

Incident Shock Experiments with Fe and Pb. Figure 2 shows a typical set of turbidity traces for a single concentration of $Fe(CO)_5$, 0.74% in Ar. The four records are for the same initial sample pressure but for differing shock strengths. Shock arrival is indicated by the step function in the pressure recorded by the gauge in the plane of the observation window center. At low temperatures (high supersaturations), $(I_0 - I)$ shows a very rapid increase due to attenuation by the condensate, then a flat plateau. Freund[4] and Homer[9] demonstrated that "plateauing" occurs when all the monomer had entered the condensed phase. As the shock temperature was increased, the level of supersaturation decreased, and the rate of condensation slowed, indicated by the longer time for the $(I_0 - I)$ trace to attain the plateau. Eventually a temperature and a supersaturation level was reached where no condensation appeared within 500 μs past shock arrival. This condition is identified as the critical supersaturation ratio, S_c, at the temperature T. Its magnitude is given by the ratio of the calculated pressure of metal vapor behind the incident shock to the equilibrium vapor pressure at that shock temperature. The approach to S_c was repeated several times, starting either with a new initial total pressure of the same mixture or at the same initial pressure but with new concentrations. Thus, we were able to collect critical supersaturation data over a extended range of temperatures.

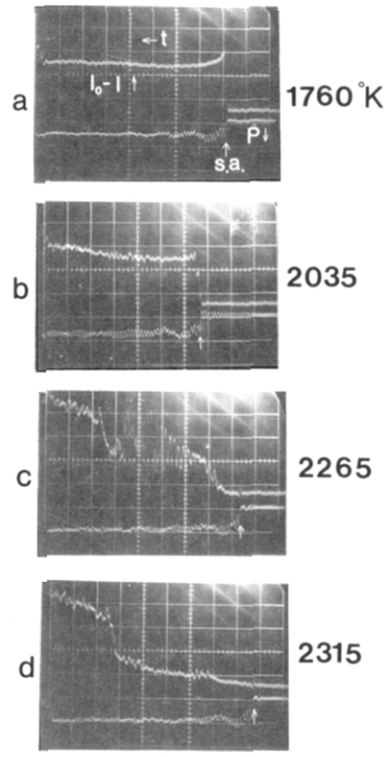

Figure 2. A typical set of traces for the incident shock experiments, showing pressure and transmitted intensity. For this sequence, 0.74% $Fe(CO)_5$ in Ar was subjected to increasing shock Mach numbers by increasing the diaphragm thickness, and thus the driver pressure. Shock arrival is indicated by the arrow (↑); lab time scale is 100 μs/division. Light extinction shows a rapid rise to a plateau, at the lower temperatures, due to very rapid condensation. As the supersaturation ratio is decreased the rise to the plateau becomes gradual. The critical condition was interpolated as being midway between 2265 and 2315 K. The fluctuating turbidity during later times in these two traces is probably due to diffusion of large particles into the narrow laser beam.

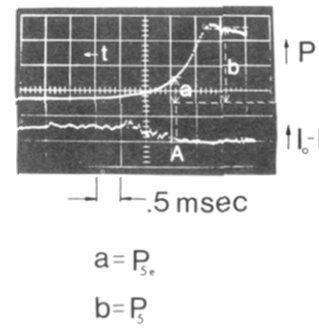

Figure 3. A typical oscilloscope record for a reflected shock experiment. Lab time scale = 0.5 ms/division.

Reflected Shock Experiments with Bi. A typical pressure–intensity record for a reflected shock in Bi vapor (diluted in Ar) is shown in Figure 3. The turbidity trace shows no evidence of condensation in the incident and reflected shock regimes, as expected, since the incident shock temperature is too low for rapid TMB decomposition while the reflected shock temperature is high enough to generate an undersaturated state. The decay of the pressure trace indicates the arrival of the expansion wave which cools the gas via an adiabatic expansion. Thus a temperature is reached such that the Bi vapor attains critical supersaturation, and begins to condense. That point appears in the turbidity trace where the laser beam

TABLE II: Physical Data for Fe, Bi, and Pb

	Fe	Bi	Pb
Surface tension $\sigma(T)$, erg cm^{-2}	2187-0.22T K	418-0.07T K	514-0.09T K
Liquid density $\rho(T)$, g cm^{-3}	8.5-8.5 × 10^{-4}T K	10.7-1.2 × 10^{-3}T K	10.7-1.3 × 10^{-3}T K
Melting point-boiling point, K	1808-3273	544-1723	600-1893
ΔH_{vap}, kcal/mol	84.6	42.6	42.0
Crystal structure	bccub	O_h	fccub

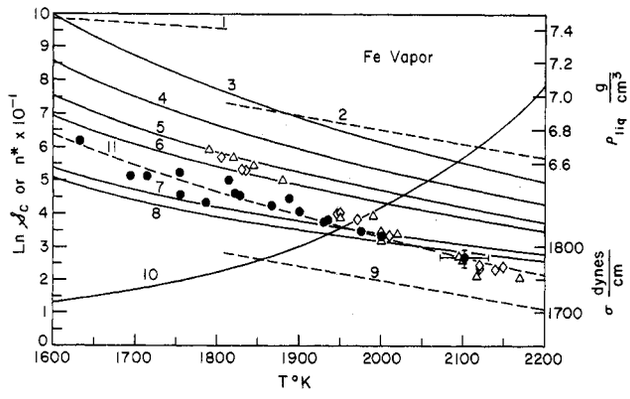

Figure 4. $S_c(T)$ for Fe. The curves superposed on the experimental points show theoretical values, according to the following key: (1) metal solid density (measured); (2) metal liquid density (measured); (3) classical theory with $J = 10^{16}$ cm^{-3} s^{-1}; (4) classical theory with $J = 10^{12}$; (5) classical theory with $J = 10^{8}$; (6) classical theory with $J = 10^{5}$; (7) Lothe-Pound theory with $J = 10^{16}$; (8) Lothe-Pound theory with $J = 10^{12}$; (9) metal liquid (bulk) surface tension (measured); (10) critical size cluster; (11) best fit exponential to data points of this work (●). (◇) Kung's results from turbidity data in the expansion wave; (△) Kung's results from black-body emission data.

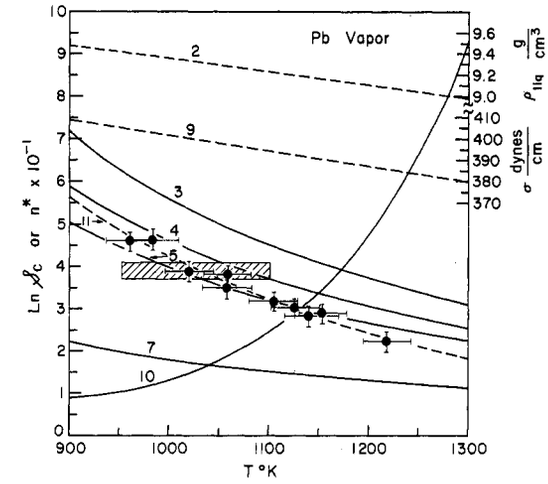

Figure 5. $S_c(T)$ for Pb. The key is the same as Figure 4.

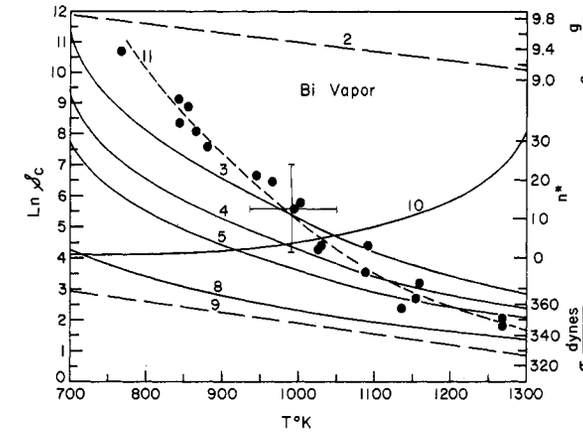

Figure 6. $S_c(T)$ for Bi. The key is the same as for Figure 4.

is first attenuated (point A in Figure 3); it is identified as the critical supersaturation ratio at the temperature T_{5e}, calculated from eq 4. The ratio P_5/P_{5e} was measured directly from the recorded output of the transducer. To obtain data over a wide range of temperatures we had only to vary (judiciously) the following: diaphragm thickness, initial test section pressure, sample concentration, and molecular weight of the driver gas. The shock tube became "detuned" (i.e., the pressure history in the reflected and expansion waves showed some unwanted structure) when the above parameters were changed too drastically. The tube was then retuned by adjusting the length of the driver section for each temperature range.

We investigated the possibility of applying these techniques to the study of condensing silicon, using the precursors $Si(CH_3)_4$ and SiH_4. At incident shock temperatures (1000–1500 K), a 1% sample of TMS did not decompose fast enough to produce a critically saturated metal vapor. However, the absorption signal at 6328 Å showed an initial rise and return to zero (within 50 μs) which we attributed to a short lived absorbing intermediate in the decomposition process. A 1% sample of silane did show evidence of decomposition under these conditions, to form a critically supersaturated vapor. The attenuation signal showed a rise and plateau, characteristic of condensation. We conclude that silane is a good candidate for a source of silicon atoms.

Comparison of the Experimental Results with Theory

The "classical" and Lothe-Pound (LP) predictions of $S_c(T)$ for Fe, Pb, and Bi are compared with our experimental points in Figures 4–6. A summary of the values for the bulk surface tension, σ, and the bulk (liquid) density, ρ, used in these calculations is given in Table II. Since no data are available for the temperature dependence of the surface tension of Fe(l), Kung and Bauer[1] estimated $\sigma(T)$ from surface entropy values; the same functional dependence was assumed here. In the case of iron, the experimental data spanned the bulk melting point. We extrapolated the values of $\sigma(T)$ and $\rho(T)$ from the liquid region into the solid region. In our search for the "best fit", the calculations were repeated for various values of the condensation current, J (number of nuclei generated per second per centimeter^3). For the LP case, the value of the "replacement factor", q_{rep}, was set equal to unity. The moment of inertia of an $n$mer, I_n, inserted in the rotational partition function was assumed to be that for a sphere of uniform density

$$I_n = \frac{2}{5}nmr^2 = \frac{2}{5}nm\left(\frac{3n}{4\pi\rho_n}\right)^{2/3} \quad (5)$$

where m is atomic mass and ρ_n is the number of atoms per unit volume. In the classical BD theory $S_c(T)$ and J are related via a cubic equation

$$\alpha(T)\ln^3 S - \ln J \cdot \ln^2 S - \beta(T) = 0 \quad (6)$$

where $\alpha(T)$ and $\beta(T)$ are collections of temperature dependent parameters. In the LP formulation an iterative process must be used to complete the calculation.

Iron Vapor. Inspection of Figure 4 shows that for reasonable values of the condensation current ($10^5 \leq J \leq 10^{16}$ s^{-1} cm^{-3}), the experimental points exhibit a temperature dependence which is steeper than predicted by either theory, although they are closer to the LP envelope of curves than to the BD curves. Empirically, they are well expressed by

$$\ln S_c = 77.88 \exp[-1.57 \times 10^{-3} T \text{ K}] \quad (7)$$

with a correlation coefficient of 0.95. The results of Kung and Bauer were also included in Figure 4. Their values show a somewhat steeper temperature dependence, since their points superpose the present set for $T > 1900$ K but rise above them for lower temperatures. Note that they used the onset of black body radiation, rather than turbidity to ascertain the start of avalanche condensation, and operated with reflected shocks rather than incident shocks. On the whole, the agreement is very good. The deviation at lower temperatures may be due to the relatively large uncertainty in estimating the temperatures in the expansion wave.

We estimated the length of the error bars for the present data by noting that the largest single source of error in the turbidity experiments is the shock temperature. The maximum uncertainty in measuring the shock speed is ± 0.02 mm μs^{-1}. To minimize the error in reading the finite width of the raster pulse measurements were made from peak to peak. This gave us a random error of about ± 30 K in the calculated equilibrium temperatures. Because of the exponential temperature dependence of the equilibrium vapor pressure, the uncertainty in shock temperature results in maximum uncertainty in ln S_c of ± 0.25. The experimental uncertainty is therefore insufficient to bring our data down to the theoretical predictions.

It is interesting to note that Kung and Bauer estimated cluster temperatures to be 50–150 K higher than the ambient gas temperature due to the heat of condensation. The abscissa scale in Figures 4–6 should be T_{cluster} since this determines the evaporation rate. For all the metals studied, the disparity between experiment and theory would be enhanced.

The condensation current, J, is an unmeasurable quantity in this experiment. One may inquire whether it is possible to fit the theoretical curves to the experimental points by using J as an adjustable parameter. It is evident that the theoretical calculations are insensitive to value of J; for example, we must set $J \gtrsim 10^{24}$ s^{-1} cm^{-3} in order that the LP theory fit the lower temperature data. This is larger than any conceivable nucleation rate under the present conditions. At the other end, to fit the high temperature range requires $J \lesssim 1$ s^{-1} cm^{-3}. This is obviously too slow, since we observed complete condensation of all the Fe monomer within 200 μs.

Since the theoretical curves are sensitive to the assumed value of the surface tension one can force fit the LP curves to the experimental points by selecting a temperature dependent surface tension. Curve 11 in Figure 4 shows the fit obtained by assuming the function

$$\sigma(T) = 4059 - 1.16T \text{ K, erg cm}^{-2} \quad (8)$$

The published surface tension values for Fe(l) at 1825 K[12,13] range from 1788 to 1865 erg cm^{-2}; eq 8 gives $\sigma = 1942$ erg cm^{-2}, which is only 0.4% above the largest experimental value. However, the temperature coefficient of 1.16 is much too large; similar factors for Bi and Pb were experimentally determined as 0.07 and 0.09, respectively. Also, since $\sigma \to 0$ as the temperature $T \to T_c$, one is led by eq 8 to a critical temperature for Fe of 3500 K, only 1700 K above its melting point, obviously much too low.

Note also that there is no break in the experimental data at the bulk melting point (1808 K). The clusters are generated with short-range order, as supercooled liquids, well above the nucleation temperature for transition to the solid phase.

Pb Vapor. Figure 5 shows the experimental points and the corresponding theoretical calculations for lead. Due to kinetic constraints on the rate of TML decomposition all the runs were made at temperatures greater than 980 K. As in the case of Fe vapor, the experimental points exhibit a temperature dependence which is too steep. The data were empirically fitted to an exponential function (curve 11)

$$\ln S_c = 69.4 \exp(-2.79 \times 10^{-3} T \text{ K}) \quad (9)$$

In contrast to the Fe data, the experimental values for Pb are close to the prediction of the classical BD theory with $J = 10^8$ s^{-1} cm^{-3}. The uncertainty in the shock temperature leads to error bars about equal to those for Fe vapor, but they were insufficient to explain the observed deviations from theory. In this case, force fitting the experimental data to the BD curve, using J as a parameter, leaves it within reasonable bounds.

The results of Homer and Hurle[9] are shown in Figure 5 as the shaded area. They did not find a temperature dependence for the critical supersaturation ratio over the range 950–1100 K. The center of the shaded envelope straddles our curve. One possible explanation for their temperature independence is that they calculated the shock temperature inserting the thermodynamic functions solely for the inert gas diluent. There is a substantial difference ($\approx$100 K) between the calculated frozen and equilibrium temperatures. Due to the exponential temperature dependence of the equilibrium vapor pressure, Homer's calculated critical supersaturation ratios could be sufficiently changed to show the expected temperature effect.

Bi Vapor. Bismuth vapor has a unique feature in that the gas in equilibrium with the liquid contains a substantial concentration of dimers (Figure 1). Katz et al.[14] state that the corresponding definition of supersaturation ratio for a monomer–dimer equilibrium is

$$2\text{Bi(g)} \rightleftarrows \text{Bi}_2\text{(g)} \qquad K \equiv P_{\text{Bi}_2}/P_{\text{Bi}}^2 \quad (10)$$

$$S = (P_1 + P_2)/(P_{1\text{eq}} + P_{2\text{eq}}) = (P_1 + P_1^2 K)/(P_{1\text{e}} + P_{1\text{e}}^2 K) \quad (11)$$

This assumes that the distribution of dimers in the metastable regime is governed by the same equilibrium constant as for the undersaturated gas.

The results for Bi are shown in Figure 6. These data, which show the largest deviation from the theoretical predictions, are well represented by the exponential function

$$\ln S_c = 148 \exp[-3.39 \times 10^{-3} T \text{ K}] \quad (12)$$

with a correlation coefficient $r = 0.98$. For reflected, as well as for incident shock experiments, the largest uncertainty is due to the estimation of the temperature. We measured the incident shock speed and used only the initial pressure and the concentration of the sample as input to the NASA program. Since the reflected shock wave passes through the incident shock heated gas, conditions in the reflected shock are determined by the state of the previously shocked gas. Unfortunately, the NASA program was formulated for calculating reflected shock conditions for the extremes, either complete thermal

equilibrium or "frozen chemistry" in the incident shock. The reflected shock temperature, therefore, depends on whether the incident shock heated gas was thermally equilibrated. This, in turn, depends on the residence time in the incident shock. In typical runs the incident shock residence time was not long enough for complete thermal equilibrium yet not short enough to justify the assumption of "frozen" conditions. This resulted in a larger uncertainty in the *absolute* reflected shock temperature, ±60 K. We could not alleviate this problem simply by increasing the window to endplate distance, and thus increase the incident shock residence times. In order to obtain the correct conditions in the reflected shock and subsequent expansion wave, the incident shock temperature had to be in a range such that appreciable condensation will occur. Since we wanted to minimize condensation in the incident shock regime, we kept the incident shock residence times short by keeping the window to endplate distance small.

The uncertainty in the temperature results in an *absolute* uncertainty in ln S of ±1.5 for the entire experimental temperature range. Nevertheless the uncertainty is insufficient to account for the steepness of the T dependence, or remove the deviation between the low temperature experimental data and closest theoretical curve (BD, $J = 10^{16}$ s^{-1} cm^{-3}). A force fit, using J as a parameter, results in an unreasonably large estimate for J ($\gtrsim 10^{21}$ s^{-1} cm^{-3}) in the low temperature regime.

Furthermore, although the absolute error in the temperature is relatively large, the relative temperatures are properly related. For this reason, we believe that the observed temperature dependence is reliable.

Conclusions and Comments

We investigated the possibility that contaminants affected the nucleation process. Since the nucleation rate is a strong function of the surface tension, the presence of oxygen at sufficient levels could lower the surface tension of the molten metals and thereby increase the nucleation rate. A mass spectrum was taken of the experimental mixtures of Ar + $Fe(CO)_5$; no O_2 was introduced during sample preparation, and the level of oxygen was *less than* 1% of the $Fe(CO)_5$ concentration. The measured outgassing-leak rate of the shock tube was less than 0.5 mTorr/min. A maximum of 2 min elapsed between the time the sample was introduced to the shock tube and diaphragm rupture. Thus, approximately 0.2 mTorr of O_2 could have been introduced. Since the sample typically contained 250 mTorr of the metal carrier the maximum *relative* oxygen concentration was 0.1%. To prove that this level of contamination had no effect on these experiments, a mixture of 0.5% $Fe(CO)_5$ and 0.005% O_2 was prepared (10 times the maximum O_2 contamination expected). Turbidity data from this sample were indistinguishable from our previous results. The presence of dust in the shock tube might also affect the nucleation rate. A series of turbidity runs were made on a 0.5% sample of $Fe(CO)_5$ that had passed through a 250-Å pore size Millipore filter prior to injection into the clean shock tube. Again, no differences were discernable. An additional argument against spurious dust affecting our S_c values is the overall consistency of our data. The runs were made in a random sequence with respect to shock temperatures, yet they fall on a smooth curve. Contaminations by either ions or dust would have resulted in considerable scatter.

To demonstrate that the incident and reflected shock experiments gave the same results, we ran several reflected shocks for Pb and for Fe. The critical supersaturations determined by this method agreed within 10% with the incident shock results.

We conclude the following for iron: (1) The experimental data do not fit either the LP or BD prescriptions, but they lie closer to the LP curves. (2) The uncertainty inherent in our data and its analysis is insufficient to account for these deviations. (3) A force fit of the LP theory to the experimental points is possible using a modified surface tension function. However, the deduced function has an unreasonable temperature dependence. The classical BD theory does account for our data on Pb condensation, provided one uses a temperature dependent critical nucleation rate. Finally for Bi, our data lie closer to the classical theory prediction than to the LP, but no satisfactory fit to the data is possible. In view of the concurrent ambiguities in J_{critical} and $\sigma(T)$, one may question whether the determination of $S_c(T)$ can provide a meaningful test of the classical theories of condensation.

References and Notes

(1) R. T. V. Kung and S. H. Bauer, "Eighth International Shock Tube Symposium–Proceedings", Chapman and Hall, London, 1971.
(2) J. B. Homer, "Eighth International Shock Tube Symposium–Proceedings", Chapman and Hall, London, 1971.
(3) H. C. van de Hulst, "Light Scattering by Small Particles", Wiley, London, 1957.
(4) H. Freund, Ph.D. Thesis, Cornell University, August, 1975.
(5) E. F. Greene and J. P. Toennies, "Chemical Reactions in Shock Waves", Academic Press, New York, N.Y., 1964.
(6) S. Gordon and B. McBride, *NASA Spec. Publ.*, **No. 273** (1971).
(7) S. Matsuda, *J. Chem. Phys.*, **57**, 807 (1972).
(8) R. Hultgren, R. L. Orr, P. D. Anderson, and K. K. Kelley, "Selected Values of Thermodynamic Properties of Metals and Alloys", Wiley, New York, N.Y., 1963.
(9) J. B. Homer and I. R. Hurle, *Proc. R. Soc. London*, **61**, 327 (1972).
(10) S. J. Price and A. F. Trotman-Dickenson, *Trans. Faraday Soc.*, **54**, 1630 (1958).
(11) P. M. Jeffers, *J. Phys. Chem.*, **76**, 2829 (1972).
(12) T. J. Hugel, Ed., "Liquids: Structures, Properties, Solid Interactions", Elsevier, New York, N.Y., 1965.
(13) C. A. Hampel, Ed., "Encyclopedia of the Chemical Elements", Reinhold, New York, N.Y., 1968.
(14) J. L. Katz, H. Saltsburg, and H. Reiss, *J. Colloid Interface Sci.*, **21**, 560 (1966).